THE JOURNAL OF PHYSICAL CHEMISTRY LETTERS
A JOURNAL OF THE AMERICAN CHEMICAL SOCIETY

pubs.acs.org/JPCL Letter

Influence of Mode-Specific Excitation on the Nonadiabatic Dynamics of Methyl Nitrate (CH_3ONO_2)

Juanjuan Zhang, Jiawei Peng, Yifei Zhu, Deping Hu,* and Zhenggang Lan*

Cite This: J. Phys. Chem. Lett. 2023, 14, 6542−6549 Read Online

ACCESS | Metrics & More | Article Recommendations | Supporting Information

ABSTRACT: The impact of mode-specific vibrational excitations on initial-preparation conditions was studied by examining the excited-state population decay rates in the nonadiabatic dynamics of methyl nitrate (CH_3ONO_2). In particular, exciting a few specific modes by adding a single quantum of energy clearly decelerated the nonadiabatic dynamics population decay rates. The underlying reason for this slower population decay was explained by analyzing the profiles of the excited-state potential energy surfaces in the Franck−Condon regions and the topology of the S_1/S_0 conical intersection. This study not only provides physical insights into the key mechanisms controlling nonadiabatic dynamics but also shows the possibility of controlling nonadiabatic dynamics via mode-specific vibrational excitations.

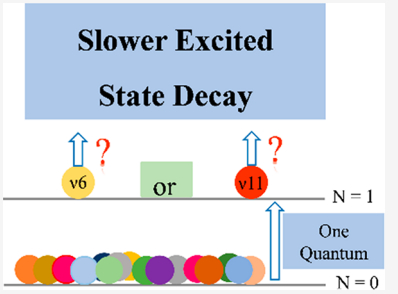

Nonadiabatic dynamics are common in photoinduced processes within polyatomic systems. In recent decades, considerable efforts have been devoted to finding possible methods of controlling nonadiabatic processes at conical intersections (CIs).[1−11] Among them, one promising idea is to employ mode-specific vibrational excitation, i.e., the initial preparation of particular vibronic states to influence the nonadiabatic dynamics, such as the adjustment of the excited-state population decay rate and the control of photoreaction products.[2,3,12−19]

At the atomic level, ultrafast nonadiabatic dynamics is normally governed by the excited-state potential energy surfaces (PESs), active reaction coordinates, the topology of the CI branching space spanned by the **g**−**h** vectors, and damping effects caused by many additional environmental degrees of freedom. Therefore, suitably adjusting these factors could modify the nonadiabatic dynamics of a system, enabling the control of the corresponding photoreactions. Since many nonadiabatic dynamics are relevant to several particular nuclear motions, some studies have suggested that mode-specific vibrational excitations in the initial preparation could control photoreactions.[20−27] For instance, in ammonia, different vibrational mode excitations lead to photoinduced dissociation dynamics with distinct products.[28,29] Regarding the well-known $\pi\sigma^*$-driven hydrogen dissociation of pyrrole, phenol, and their derivatives, Domcke and co-workers[26,27,30−32] showed that tuning mode excitations accelerated the nonadiabatic dynamics, while coupling mode excitations had a strong impact on the branching ratio of different channels. Ohtsuki and co-workers[13] further demonstrated the possibility of controlling photoinduced products using optimal laser fields, wherein particular vibronic states are prepared and the geometric phase is an important factor. Guo and co-workers[12] performed systematic studies on the role the geometric phase in the nonadiabatic tunneling dynamics via $\pi\pi^*-\pi\sigma^*$ CIs from initial conditions with mode-specific vibrational excitations. Crim and co-workers[14] confirmed that pre-excitation of the OH stretching mode significantly impacts the nonadiabatic pathway of the phenol photolysis. Mode-specific excitation also significantly influences nonadiabatic dynamics in photoisomerization dynamics. Gordon, Martínez, and co-workers[33] showed that the photoinduced isomerization of *trans*-azomethane can be modified via the central C−N═N−C torsional mode excitations. These studies have all demonstrated that nonadiabatic dynamics may be modified by mode-specific excitation. Certainly, energy transfers from a few active coordinates to many other nonphotoactive degrees must be avoided, since such damping effects take the excess energy in the active modes and eliminate the possibility of reaction control. Therefore, small-molecule systems are ideal candidates for controlled studies. The smallest alkyl nitrate, methyl nitrate (CH_3ONO_2), has a simple molecular geometry. This study examined the possibility of controlling the excited-state lifetime in the nonadiabatic dynamics of a CH_3ONO_2 system.

The photochemistry of CH_3ONO_2 has been widely studied due to its importance in environmental and atmospheric sciences.[34−39] Experimental studies have shown the extensive excitation band of CH_3ONO_2 in the high-energy domain with a very long tail in the low-energy domain in the absorption spectra.[40,41] The photolysis of CH_3ONO_2 yields different

Received: March 10, 2023
Accepted: July 7, 2023
Published: July 14, 2023

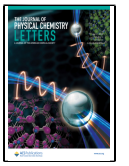

https://doi.org/10.1021/acs.jpclett.3c00664
J. Phys. Chem. Lett. 2023, 14, 6542−6549

photoproducts, namely, $CH_3O + NO_2$, $CH_3O + NO + O$, and $CH_3ONO + O$, with their ratios dependent on the excitation wavelength. Theoretical calculations have suggested that CIs are essential in the photolysis dynamics of CH_3ONO_2 and similar systems.[38,39,42−44] Using on-the-fly surface hopping dynamics, we previously showed that the ultrafast excited-state decay dynamics of CH_3ONO_2 via S_1/S_0 CIs occur during photolysis.[45] In addition, a few nuclear motions, such as pyramidalization at the N atom, are critical in excited-state decay dynamics.

This study examined the initial-preparation dependence of the excited-state lifetime in the nonadiabatic dynamics of a CH_3ONO_2 system. We showed that mode-specific vibrational excitation could influence nonadiabatic dynamics. In particular, for some specific modes, single quantum−vibrational excitations appeared to decelerate the excited-state population decay dynamics. The underlying reason is relevant to the PESs in the Franck−Condon (FC) region and the topologies of the involved CIs. Thus, this work not only provides a valuable understanding of the mechanisms of controlling nonadiabatic dynamics via mode-specific vibrational excitations but also suggests a possible control strategy for further experimental studies.

We chose a few important modes to examine the influence of mode-specific excitations on nonadiabatic dynamics. First, the modes with large vibronic couplings were selected, as they may impact the photoinduced dynamics starting from the FC region. Therefore, all vibrational modes at the ground-state minimum-energy geometry (S_0-min) were obtained at the B3LYP/6-311+G* level[46−49] using the Gaussian 16 software package.[50] The gradient of the first excited state (S_1) at S_0-min was calculated at the XMS-CASPT2 level.[51−53] The linear vibronic coupling term κ_i for each mode was calculated using this information by projecting the S_1 gradient from Cartesian coordinates to dimensionless normal coordinates (Table S1 in the Supporting Information). Two modes, $\nu 7$ and $\nu 11$ (Figure 1), with large vibronic coupling strengths ($|\kappa_i/\omega_i| > 1$) were

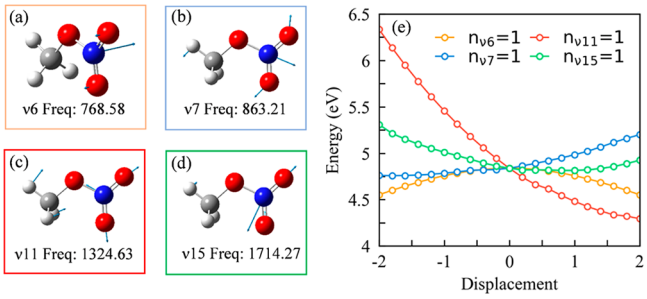

Figure 1. Selected vibrational modes (a−d) [unit of frequency: cm^{-1}] and their S_1 PES (e) in the FC region.

selected; this is discussed further below. Second, we previously found that S_1/S_0 CIs are relevant to the nonadiabatic dynamics of CH_3ONO_2.[45] In particular, the CI with a short CH_3O-NO_2 distance and strong pyramidalization at the N atom was the most important because many first hops from the S_1 to S_0 states ($S_1 \rightarrow S_0$ hops) take place in this CI seam region. Therefore, we calculated the orthogonal gradient difference vector **g** and interstate coupling vector **h** at this important CI (Table S2 and further discussions in the Supporting Information).[54] On this basis, we computed the angle between the dimensionless normal coordinate of each mode and the orientation of the **g** or **h** vector, which provided the contribution of each mode in the CI branching space (Tables S3 and S4). When this angle differs from 90° by more than 25°, the corresponding mode contributes to the **g** or **h** vector of the CI. According to this rule, we added modes $\nu 6$ and $\nu 15$. Based on the above two criteria, four modes ($\nu 6$, $\nu 7$, $\nu 11$, and $\nu 15$) were selected.

To obtain the proper initial conditions of the trajectory surface hopping dynamics that mimic the excitation of these vibrational modes, we used the action-angle sampling for generating the initial coordinates and velocities.[55,56] Here, we only considered the simplest condition wherein only one quantum was added on a single mode, with the other modes remaining at the lowest level.

Based on these initial conditions, the nonadiabatic dynamics of CH_3ONO_2 were simulated using on-the-fly surface hopping dynamics with Tully's fewest-switches algorithm[57] at the XMS-CASPT2 level. All nonadiabatic dynamics simulations were performed using JADE-NAMD code,[56] which contains an interface between the nonadiabatic dynamics and the electronic-structure calculations using BAGEL.[58] In addition, the PESs along the dimensional normal coordinates were built at the XMS-CASPT2 level. All computational setups were consistent with our previous work[45] and described in the Supporting Information.

When the nonadiabatic dynamics began from the lowest vibrational level of the electronic ground state, approximately half of the trajectories decayed to S_0 within 55 fs and about 70% of trajectories decayed to S_0 within 120 fs (Figure 2). This was consistent with the data of our previous study, which used the Wigner function to perform the initial sampling for nuclear degrees of freedom. Three S_1/S_0 CIs were responsible for the nonadiabatic dynamics of CH_3ONO_2, namely, CI_{10}-I, CI_{10}-II, and CI_{10}-III (Figure S1). Among these, CI_{10}-I and CI_{10}-II had long CH_3O-NO_2 distances (>3.0 Å) with different O−N−O angles (133° and 110°, respectively). The system at both CIs could be roughly viewed as two radical fragments ($CH_3O + NO_2$). CI_{10}-III was characterized by a short CH_3O-NO_2 distance, strong pyramidalization at the N, and torsional motion along the N−O bond. Starting with CI_{10}-III, we modified the torsional angle of the N−O bond as another initial geometry and performed a new CI optimization while constraining the torsional angle. This resulted in a near planar geometry at this CI seam, with a slightly torsional N−O bond (173°). This was labeled as CI_{10}-III-P and its energy was 0.2 eV higher than that of CI_{10}-III. This CI geometry was located since most structures of the first $S_1 \rightarrow S_0$ hops occur near CI_{10}-III-P rather than CI_{10}-III and we observed no significant torsional motion at these hops (Figure S1a). After most of the trajectories underwent their first $S_1 \rightarrow S_0$ hops in the CI_{10}-III seam region, many of them jumped back to the S_1 state. After several hops between S_0 and S_1 (Figure S1a,b), the system finally moves to its dissociation limit.

Next, we examined the time-dependent electronic population dynamics starting from different initial conditions [Figure 2(a-1)−(d-1)]. On adding one quantum of energy to modes $\nu 7$ and $\nu 15$, the population dynamics remained similar while the S_1 states had slightly shorter lifetimes [Figure 2(b-1),(d-1)]. The slight acceleration of the nonadiabatic decay dynamics can be easily explained by the slight increase in the total energy of the system due to the addition of one quantum to the chosen mode. However, mode-specific vibrational excitations in modes $\nu 6$ and $\nu 11$ slow the nonadiabatic decay

https://doi.org/10.1021/acs.jpclett.3c00664
J. Phys. Chem. Lett. 2023, 14, 6542−6549

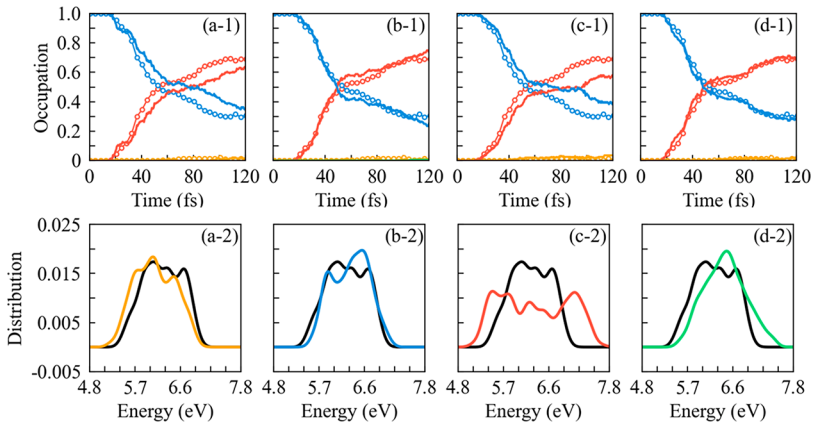

Figure 2. Time-dependent average fractional occupations in the nonadiabatic dynamics of CH_3ONO_2 simulated for mode-specific vibrational excitations: (a-1) $n_{\nu 6} = 1$, (b-1) $n_{\nu 7} = 1$, (c-1) $n_{\nu 11} = 1$, and (d-1) $n_{15} = 1$. The open circles represent $n_\nu = 0$, and the solid lines represent the different mode excitation cases. The red, blue, orange, and green lines represent the S_0, S_1, S_2, and S_3 states, respectively. The total energy (sum of the kinetic and S_1 potential energies) of 200 initial structures under different sampling conditions is also included: (a-2) $n_{\nu 6} = 1$ (orange line), (b-2) $n_{\nu 7} = 1$ (blue line), (c-2) $n_{\nu 11} = 1$ (red line), and (d-2) $n_{\nu 15} = 1$ (green line), with the black line representing $n_\nu = 0$.

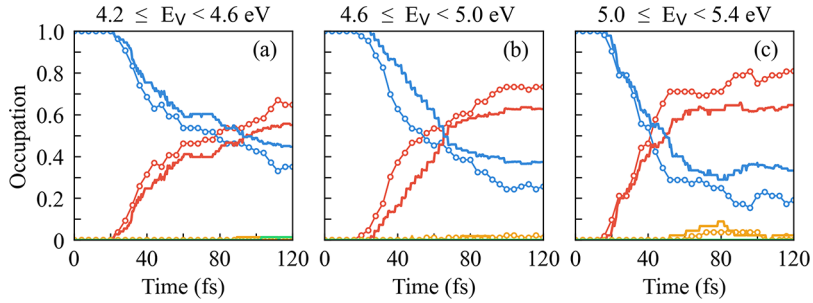

Figure 3. Time-dependent average fractional occupations in the nonadiabatic dynamics of CH_3ONO_2 simulated for mode-specific vibrational excitation within different energy windows. In all panels, E_v represents the vertical excitation energy of the initial structures. The open circles represent $n_\nu = 0$, and the solid lines represent $n_{\nu 11} = 1$.

dynamics, as demonstrated by their respective S_1 populations [Figure 2(a-1),(c-1)]. Without vibrational excitations, approximately 50% of the trajectories decayed to the S_0 state at 55 fs. After adding one quantum to each of these two modes, approximately half of the trajectories remained in the S_1 state at around 80 fs, resulting in an approximately 50% slower decay than that of the nonexcited case. This counterintuitive result invoked a very interesting question: Why does the S_1 population become slower in the current system when one quantum is added to mode $\nu 6$ or $\nu 11$?

To answer this question, we first examined the total energy distribution of the initial sampled structures under different mode-specific excitation conditions [Figure 2(a-2)−(d-2)]. The total energy was the sum of the kinetic and S_1 potential energies for each sampled geometry, which also corresponded to the energy at time zero in the nonadiabatic dynamics. For $n = 1$ excitations of modes $\nu 6$ and $\nu 11$, the distribution probabilities at the low-energy domain increased with respect to the same modes without vibrational excitations (Figure 2). This difference was particularly significant for $n_{\nu 11} = 1$. In the case of $n_{\nu 6} = 1$, the difference was not pronounced but still visible.

For physical insights into the existence of the low-energy portions in the initial conditions of the nonadiabatic dynamics, we examined the PESs along these modes in the FC region (Figure 1e). Mode $\nu 11$ displayed a strong gradient along this motion due to its large vibronic coupling strength (Table S1), which resulted in the low-energy portions in the initial sampled geometries.

The pyramidalization at the N atom is the dominant motion for mode $\nu 6$, and this motion is also an important driving factor for the system to access the CIs. Importantly the displacement of this mode has two equivalent orientations. Therefore, the S_1 PES along mode $\nu 6$ shows a flat region at S_0-min and the zero vibronic coupling strength is given (Table S1), which then quickly decreases with the displacement along both directions of motion of this mode. This indicates that the excitation of this mode reduces the potential energy of S_1. Therefore, the low-energy part becomes more prominent in the total energy distribution, although this change may not be significant. In brief, the low-energy portion brought about by the excitation of mode $\nu 6$ was confirmed on examining the S_1 PES profile at the FC region. Although the difference in the distributions under both initial conditions was not significant, i.e., the low-energy part (<5.7 eV) for $n_{\nu 6} = 1$ was approximately 10% more than that of $n_{\nu 6} = 0$, this difference is sufficient to explain the slower S_1 population decay dynamics for $n_{\nu 6} = 1$.

Vibrational excitations of modes $\nu 6$ and $\nu 11$ resulted in the low-energy parts contributing more to the initial condition, which led to more trajectories taking longer to access the CI seam. This was confirmed by the mean time of the first $S_1 \rightarrow S_0$ hops (Table S5) and the fewer hops in the short-time domain (Figure S2) compared with the cases without vibrational excitation. After the mode-specific excitation of these two

https://doi.org/10.1021/acs.jpclett.3c00664
J. Phys. Chem. Lett. 2023, 14, 6542−6549

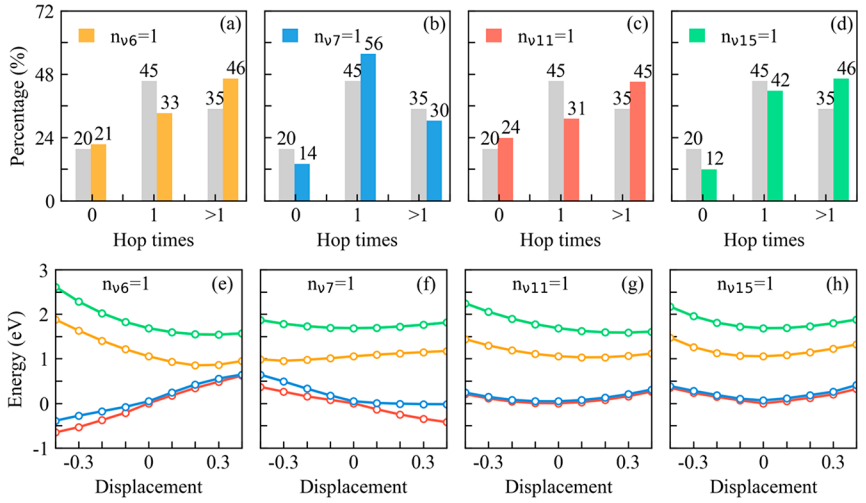

Figure 4. Ratios of different types of trajectories with no hop, a single hop, and multiple hops in the mode-specific excitation of nonadiabatic dynamics over 120 fs (a–d), with the gray bar representing $n_\nu = 0$. The PESs along the specific modes near CI_{10}-III-P (with the energy set to zero) are shown in (e)–(h), with the red, blue, orange, and green lines representing the S_0, S_1, S_2, and S_3 states, respectively.

modes, the mean time of the first $S_1 \rightarrow S_0$ hops becomes longer. These factors decelerated the S_1 population decay. Overall, these results indicate that a low initial energy is the major factor contributing to a slower population decay after $n_{\nu 6} = 1$ and $n_{\nu 11} = 1$ mode-specific excitations.

To further understand the influence of the initial excitation on nonadiabatic dynamics, we evaluated different excitation energy windows.[59−61] As an illustrative example, only the excitation of mode $\nu 11$ was investigated. Transition energy windows were used to determine the influence of photoexcitation within particular transition energy domains on nonadiabatic dynamics. The three approximate excitation energy windows used were 4.2–4.6, 4.6–5.0, and 5.0–5.4 eV, and their population dynamics are shown in Figure 3. The excited-state S_1 population decay accelerated with increasing excitation energies for both $n_{\nu 11} = 0$ and $n_{\nu 11} = 1$ (Figure 3). For this mode, high excitation energies normally indicate large geometrical distortions. Considering the PES shape along this normal coordinate, these geometries displayed a large potential energy that drove the system to access the CI quickly and resulted in a faster population decay. Within the same energy windows, the single quantum excitations of mode $\nu 11$ decelerated the S_1 population decay. Exploring the different dynamics features with and without mode-specific excitations within the same excitation energy window required a detailed examination of the trajectory propagation.

An examination of the trajectory propagation revealed that several hops between S_1 and S_0 may exist in the nonadiabatic dynamics of CH_3ONO_2, as shown in Figure 4a–d and Figure S2b. Similar features of multiple hops were also observed in the nonadiabatic dynamics within different excitation energy windows (Table S6). Notably, we observed many successful and frustrated hops from S_0 to S_1. These multiple hops in the trajectory propagation are relevant to the topology of the CI seam.

One important observation was that the **g** vector was several magnitudes larger than the **h** vector at both CI_{10}-III and CI_{10}-III-P (Table S2). Since **h** was extremely short, the CI seam became (quasi)$N-1$ dimensional with a more extended state degeneracy region in the CI_{10}-III and CI_{10}-III-P regions. Such (quasi)$N-1$ dimensional degeneracy at CI has also been observed in other systems.[62,63] As both modes $\nu 11$ and $\nu 15$ are important components of **h**, the PESs of the two lowest electronic states remained nearly degenerate along these two modes (Figure 4). Both modes $\nu 6$ and $\nu 7$ contributed to **g**. The excitation of the vibrational motion along **g** should lift the state degeneracy. However, $\nu 6$ was also relevant to the **s** vector, while $\nu 7$ was perpendicular to **s**. Since **s** characterizes the CI seam direction, the energy gap of both PESs remained small along the dimensionless coordinate of mode $\nu 6$ (Figure 4). In contrast, a displacement along mode $\nu 7$ resulted in a visible energy gap between S_1 and S_0 (Figure 4).

Overall, nonadiabatic dynamics likely occur in the following manner: Initially, the system moved from the FC region to access the CI_{10}-III-P seam via strong pyramidalization of the N atom. When trajectories jump to the S_0 state, they remained in the CI_{10}-III-P region for an extended duration and could return back to the S_1 state. After several hops between S_0 and S_1, the system finally moved to the dissociation limit with the products CH_3O and NO_2. This explains why several rehops occur in the current dynamics.

Single-quantum excitations of modes $\nu 6$ and $\nu 11$ increased the number of rehops, which resulted in longer excited-state S_1 population lifetimes. The underlying reasons can be addressed by carefully analyzing the molecular motions near the CI seam. After the first $S_1 \rightarrow S_0$ hops, the trajectories remained in motion near the CI seam region, giving the possibility for $S_0 \rightarrow S_1$ rehops. However, these trajectories were rarely able to touch the exact degeneracy. Therefore, the $S_0 \rightarrow S_1$ back hops needed to overcome the small energy gaps, and their success was determined by whether the energy conservation is satisfied or not. When the kinetic energy was large enough, more successful $S_0 \rightarrow S_1$ hops took place, resulting in a slower excited-state population decay. This indicates that controlling the ratio between the successful and frustrated hops could modify the population dynamics. Using $n_{\nu 11} = 0$ and $n_{\nu 11} = 1$ as representative examples, we observed many successful and frustrated hops between the S_0 to S_1 states in the three energy windows (Table S6). In the initial condition for $n_{\nu 11} = 1$, the system had larger kinetic energies compared to the $n_{\nu 11} = 0$ case. The excessive kinetic energy for $n_{\nu 11} = 1$ allowed more trajectories to return to the S_1 state, thereby reducing the

https://doi.org/10.1021/acs.jpclett.3c00664
J. Phys. Chem. Lett. 2023, 14, 6542−6549

number of frustrated hops. This was confirmed by the reduction in the number of frustrated hops with vibrational excitation for $n_{\nu 11} = 1$ (Table S6). Consequently, the overall population decay slowed down. For similar reasons, an initial high energy also resulted in fewer frustrated hops and more successful $S_0 \rightarrow S_1$ hops, as shown in Figure 3 and Table S6.

Therefore, the existence of the $S_0 \rightarrow S_1$ rehops allows a deceleration of the population dynamics with mode-specific excitations due to the special topology of the CI seam. However, it is important to note that this effect is only a secondary reason for modifying the population decay dynamics, with the initial energy being more important. For instance, even if the dynamics in the high-energy window showed more rehops, the overall population dynamics were still faster (Figure 3 and Table S6).

Combing all of the above analyses regarding the PES at the FC regions and CI_{10}-III-P generates a complete understanding of the role of mode-specific excitations in nonadiabatic decay dynamics, which includes an interesting interplay between the two factors.

Mode $\nu 6$ shows a very small gradient at the FC region due to the symmetry. However, displacement along this mode reduced the potential energy. The positive and negative displacement directions along mode $\nu 6$ revealed a symmetrical PES curve. Its excitation could therefore push the system to acquire a lower energy and slow the nonadiabatic decay. Simultaneously, while this mode contributed to the **s** vector that characterizes the CI seam direction, it was also relevant to the **g** vector. The excitation of this mode did not result in a significant energy split due to the special topology of the involved CI. Consequently, the system remained near the quasi-degenerate region with a (quasi)$N - 1$ dimension, which resulted in many frustrated and successful $S_0 \rightarrow S_1$ hops if vibrational energy transfers were not involved. However, this explanation is highly qualitative; vibrational energy transfers occur rapidly, and such effects should be considered. We hypothesize that excitation of this mode results in a high kinetic energy in the initial samplings, which reduces the number of frustrated hops and increases the number of successful hops from S_0 to S_1. Both reasons finally decelerated nonadiabatic decay.

Although mode $\nu 7$ showed a visible gradient, its excitation did not produce more low-energy components in the initial sampling. Additionally, the motion along this mode lifted the state degeneracy in the CI_{10}-III-P region due to its strong contribution to **g**, thereby reducing the possibility of $S_0 \rightarrow S_1$ hops. Consequently, we observed no slow downs of the nonadiabatic dynamics after single quantum−vibrational excitations.

Mode $\nu 11$ displays a very strong gradient for the S_1 PES in the FC region, resulting in more low-energy components in the initial sampling. The special topology of the CI_{10}-III-P seam showed (quasi)$N - 1$ dimensions, which extended the state degeneracy. Therefore, the PESs along mode $\nu 11$ remained nearly degenerate despite this mode being relevant to the **h** vector. For reasons similar to those discussed previously, a deceleration of the nonadiabatic decay was observed. However, this effect was more pronounced here compared with that of the excitation of mode $\nu 6$. This confirms the importance of the initial energy, while the rehops only play a secondary role.

For mode $\nu 15$, the S_1 PES gradient was not strong enough in the FC region. Therefore, an excitation of this mode resulted in a large proportion of the high-energy component. Despite a large number of rehops, the overall results showed no clear impacts of the nonadiabatic dynamics. Here, the high initial energy rapidly drove the system to the CI seam, as demonstrated by the mean time of the first hop from S_1 to S_0 (Table S5). This further demonstrated the importance of the initial energy in the nonadiabatic dynamics of the current system.

All above calculations employed the surface hopping dynamics with the decoherence correction proposed by Granucci et al.[64] For validation purposes, we used an augmented fewest-switches surface hopping (A-FSSH) method developed by Subotnik, Shenvi, and co-workers[65−69] to simulate the nonadiabatic dynamics with an initial condition with and without the mode $\nu 11$ excitation ($n_{\nu 11} = 0$ and 1). As a robust approach to treat the decoherence correction in the surface hopping dynamics, the A-FSSH method was once implemented in the on-the-fly calculations by Marquetand, González, and co-workers.[70] Here our own implementation of A-FSSH dynamics follow the step-by-step tutorial instruction in ref 66. The A-FSSH simulations showed that the excitation of mode $\nu 11$ slowed the decay of the S_1 population (Figure S3). We also observed a large number of $S_0 \rightarrow S_1$ rehops (Table S6). Both surface hopping methods give consistent dynamics features. Furthermore, when considering the transition probability for selecting the initial samplings,[56] the overall features of the nonadiabatic dynamics remained similar, as shown in Figure S4.

In summary, we studied the influence of mode-specific excitations on the nonadiabatic dynamics of CH_3ONO_2. Four vibrational modes, namely, $\nu 6$, $\nu 7$, $\nu 11$, and $\nu 15$, were considered, which were relevant to the branching space of the important CI. The nonadiabatic dynamics showed a clear deceleration following the one-quantum excitation of modes $\nu 6$ and $\nu 11$, while the same excitation of modes $\nu 7$ and $\nu 15$ did not yield similar results. The underlying reason was analyzed in terms of the PES topologies at the FC region and CI seam. Mode $\nu 11$ showed a strong S_1 gradient at the FC region, and the S_1 PES decreases along two displacement directions of mode $\nu 6$. The one quantum excitation of these modes results in more low-energy components in the initial samplings. This was the major factor influencing the population decay dynamics. Simultaneously, when the trajectories moved to the CI_{10}-III-P region, many of them experienced the first $S_1 \rightarrow S_0$ hops, displayed reversed $S_0 \rightarrow S_1$ hops, showed multiple hops, and finally moved to a dissociation limit, producing $CH_3O + NO_2$. Therefore, the back hops modify the nonadiabatic decay rate. Due to the **g** and **h** vectors differing by several orders of magnitude, the state degeneracy became (quasi)$N - 1$ dimensional in the CI_{10}-III-P region, which resulted in an extended state degeneracy region along certain modes. Consequently, the excitation of some modes reduced the number of frustrated hops due to the higher kinetic energies. This resulted in more $S_0 \rightarrow S_1$ back hops that slowed the nonadiabatic decay rate. This was the secondary factor influencing the population decay rate. The interplay between the two factors finally explained why the mode-specific vibrational excitations of some modes noticeably impact nonadiabatic decay dynamics, particularly in terms of decelerating the excited-state population decay rates.

This work provides interesting results concerning the control of the nonadiabatic population decay dynamics of CH_3ONO_2 and sheds light on possible experimental studies that may be used to explore the control of the photochemistry

https://doi.org/10.1021/acs.jpclett.3c00664
J. Phys. Chem. Lett. 2023, 14, 6542−6549

of similar systems. Moreover, this work shows the complicated dependence of nonadiabatic dynamics on the FC region, initial preparations, CI topologies, and nonadiabatic transitions. This provides a valuable understanding of the influence of mode-specific excitations on the nonadiabatic dynamics of polyatomic systems.

■ ASSOCIATED CONTENT

Supporting Information

The Supporting Information is available free of charge at https://pubs.acs.org/doi/10.1021/acs.jpclett.3c00664.

Descriptions of the **g**, **h**, and **s** vectors; computational details; angles between the vibrational modes and the **g**, **h**, and **s**, vectors at CI_{10}-III-P and CI_{10}-III; geometries of optimized CIs; distributions of all the trajectory hop times; mean time of first $S_1 \rightarrow S_0$ hops from the different initial conditions; ratios of all successful $S_0 \rightarrow S_1$ rehops and frustrated hops within different energy windows; and time-dependent average fractional occupations at mode-specific vibrational excitations within three energy windows using two TSH methods (PDF)

■ AUTHOR INFORMATION

Corresponding Authors

Deping Hu − *Center for Advanced Materials Research, Beijing Normal University, Zhuhai 519087, China*; Email: depinghu@bnu.edu.cn

Zhenggang Lan − *SCNU Environmental Research Institute, Guangdong Provincial Key Laboratory of Chemical Pollution and Environmental Safety & MOE Key Laboratory of Environmental Theoretical Chemistry and School of Environment, South China Normal University, Guangzhou 510006, China*; orcid.org/0000-0002-8509-0388; Email: zhenggang.lan@m.scnu.edu.cn

Authors

Juanjuan Zhang − *SCNU Environmental Research Institute, Guangdong Provincial Key Laboratory of Chemical Pollution and Environmental Safety & MOE Key Laboratory of Environmental Theoretical Chemistry and School of Environment, South China Normal University, Guangzhou 510006, China*; orcid.org/0009-0003-3240-9257

Jiawei Peng − *SCNU Environmental Research Institute, Guangdong Provincial Key Laboratory of Chemical Pollution and Environmental Safety & MOE Key Laboratory of Environmental Theoretical Chemistry and School of Chemistry, South China Normal University, Guangzhou 510006, China*

Yifei Zhu − *SCNU Environmental Research Institute, Guangdong Provincial Key Laboratory of Chemical Pollution and Environmental Safety & MOE Key Laboratory of Environmental Theoretical Chemistry and School of Environment, South China Normal University, Guangzhou 510006, China*

Complete contact information is available at: https://pubs.acs.org/10.1021/acs.jpclett.3c00664

Notes

The authors declare no competing financial interest.

■ ACKNOWLEDGMENTS

This work was supported by NSFC projects (Grants 21933011 and 21873112) and the Opening Project of Key Laboratory of Optoelectronic Chemical Materials and Devices of Ministry of Education, Jianghan University (Grant JDGD-202216). The authors thank the Supercomputing Center, Computer Network Information Center, Chinese Academy of Sciences, and the National Supercomputing Center in SunRising-1 for providing computational resources.

■ REFERENCES

(1) Arnold, C.; Vendrell, O.; Welsch, R.; Santra, R. Control of nuclear dynamics through conical intersections and electronic coherences. *Phys. Rev. Lett.* **2018**, *120* (12), 123001.

(2) Xie, C.; Kendrick, B. K.; Yarkony, D. R.; Guo, H. Constructive and destructive interference in nonadiabatic tunneling via conical intersections. *J. Chem. Theory Comput.* **2017**, *13* (5), 1902−1910.

(3) Csehi, A.; Halász, G. J.; Cederbaum, L. S.; Vibók, Á. Towards controlling the dissociation probability by light-induced conical intersections. *Faraday Discuss.* **2016**, *194* (0), 479−493.

(4) Gu, B.; Mukamel, S. Manipulating nonadiabatic conical intersection dynamics by optical cavities. *Chem. Sci.* **2020**, *11* (5), 1290−1298.

(5) Schüppel, F.; Schnappinger, T.; Bäuml, L.; de Vivie-Riedle, R. Waveform control of molecular dynamics close to a conical intersection. *J. Chem. Phys.* **2020**, *153* (22), 224307.

(6) Abe, M.; Ohtsuki, Y.; Fujimura, Y.; Domcke, W. Optimal control of ultrafast cis-trans photoisomerization of retinal in rhodopsin via a conical intersection. *J. Chem. Phys.* **2005**, *123* (14), 144508.

(7) Geppert, D.; Hofmann, A.; de Vivie-Riedle, R. Control of a collision complex via a conical intersection. *J. Chem. Phys.* **2003**, *119* (12), 5901−5906.

(8) Alfalah, S.; Belz, S.; Deeb, O.; Leibscher, M.; Manz, J.; Zilberg, S. Photoinduced quantum dynamics of ortho- and para-fulvene: Hindered photoisomerization due to mode selective fast radiationless decay via a conical intersection. *J. Chem. Phys.* **2009**, *130* (12), 124318.

(9) González-Vázquez, J.; González, L.; Sola, I. R.; Santamaria, J. Laser control of conical intersections: Quantum model simulations for the averaged loss-gain strategies of fast electronic deactivation in 1,1-difluoroethylene. *J. Chem. Phys.* **2009**, *131* (10), 104302.

(10) *Conical Intersections I: Electronic Structure, Dynamics and Spectroscopy*l Domcke, W., Yarkony, D. R., Köppel, H., Eds.; World Scientific: Singapore, 2004.

(11) *Conical Intersections II: Theory, Computation and Experiment*; Domcke, W., Yarkony, D. R., Köppel, H., Eds.; World Scientific: Singapore, 2011.

(12) Xie, C.; Zhao, B.; Malbon, C. L.; Yarkony, D. R.; Xie, D.; Guo, H. Insights into the mechanism of nonadiabatic photodissociation from product vibrational distributions. the remarkable case of phenol. *J. Phys. Chem. Lett.* **2020**, *11* (1), 191−198.

(13) Abe, M.; Ohtsuki, Y.; Fujimura, Y.; Lan, Z.; Domcke, W. Geometric phase effects in the coherent control of the branching ratio of photodissociation products of phenol. *J. Chem. Phys.* **2006**, *124* (22), 224316.

(14) Hause, M. L.; Yoon, Y. H.; Case, A. S.; Crim, F. F. Dynamics at conical intersections: The influence of O−H stretching vibrations on the photodissociation of phenol. *J. Chem. Phys.* **2008**, *128* (10), 104307.

(15) Liu, Y.; Song, H.; Xie, D.; Li, J.; Guo, H. Mode specificity in the $OH + HO_2 \rightarrow H_2O + O_2$ reaction: enhancement of reactivity by exciting a spectator mode. *J. Am. Chem. Soc.* **2020**, *142*, 3331−3335.

(16) Xu, X.; Yang, K. R.; Truhlar, D. G. Diabatic molecular orbitals, potential energies, and potential energy surface couplings by the 4-fold way for photodissociation of phenol. *J. Chem. Theory Comput* **2013**, *9* (8), 3612−3625.

(17) Ma, J.; Li, J.; Guo, H. Tunneling facilitated dissociation to H +CO_2 in $HOCO^-$ photodetachment. *Phys. Rev. Lett.* **2012**, *109* (6), 063202.
(18) Dutkiewicz, Ł.; Johnson, R. E.; Vertes, A.; Pędrys, R. Molecular dynamics study of vibrational excitation dynamics and desorption in solid O_2. *J. Phys. Chem. A* **1999**, *103* (16), 2925−2933.
(19) Yang, K. R.; Xu, X.; Zheng, J.; Truhlar, D. G. Full-dimensional potentials and state couplings and multidimensional tunneling calculations for the photodissociation of phenol. *Chem. Sci.* **2014**, *5* (12), 4661−4680.
(20) Xie, C.; Ma, J.; Zhu, X.; Yarkony, D. R.; Xie, D.; Guo, H. Nonadiabatic tunneling in photodissociation of phenol. *J. Am. Chem. Soc.* **2016**, *138* (25), 7828−7831.
(21) Papp, D.; Li, J.; Guo, H.; Czakó, G. Vibrational mode-specificity in the dynamics of the Cl + C_2H_6 → HCl + C_2H_5 reaction. *J. Chem. Phys.* **2021**, *155* (11), 114303.
(22) Xu, X.; Zheng, J.; Yang, K. R.; Truhlar, D. G. Photodissociation dynamics of phenol: multistate trajectory simulations including tunneling. *J. Am. Chem. Soc.* **2014**, *136* (46), 16378−16386.
(23) Roberts, G. M.; Hadden, D. J.; Bergendahl, L. T.; Wenge, A. M.; Harris, S. J.; Karsili, T. N. V.; Ashfold, M. N. R.; Paterson, M. J.; Stavros, V. G. Exploring quantum phenomena and vibrational control in σ^* mediated photochemistry. *Chem. Sci.* **2013**, *4* (3), 993−1001.
(24) Ma, J.; Xie, C.; Zhu, X.; Yarkony, D. R.; Xie, D.; Guo, H. Full-dimensional quantum dynamics of vibrationally mediated photodissociation of NH_3 and ND_3 on coupled ab Initio potential energy surfaces: absorption spectra and $NH_2(\tilde{A}^2A_1)$/$NH2(\tilde{X}^2B_1)$ branching ratios. *J. Phys. Chem. A* **2014**, *118* (51), 11926−11934.
(25) Lambert, H. M.; Dagdigian, P. J. Photodissociation of CH stretch overtone excited CH_3Cl and CHD_2Cl(vCH=5): Cl spin−orbit branching and atomic fragment yields. *J. Chem. Phys.* **1998**, *109* (18), 7810−7820.
(26) Lan, Z. G.; Domcke, W.; Vallet, V.; Sobolewski, A. L.; Mahapatra, S. Time-dependent quantum wave-packet description of the $^1\pi\sigma^*$ photochemistry of phenol. *J. Chem. Phys.* **2005**, *122* (22), 224315.
(27) Lan, Z.; Domcke, W. Role of vibrational energy relaxation in the photoinduced nonadiabatic dynamics of pyrrole at the $^1\pi\sigma^*$-S_0 conical intersection. *Chem. Phys.* **2008**, *350* (1−3), 125−138.
(28) Bach, A.; Hutchison, J.; Holiday, R.; Crim, F. Competition between adiabatic and nonadiabatic pathways in the photodissociation of vibrationally excited ammonia†. *J. Phys. Chem. A* **2003**, *107* (49), 10490−10496.
(29) Hause, M. L.; Yoon, Y. H.; Crim, F. F. Vibrationally mediated photodissociation of ammonia: The influence of N−H stretching vibrations on passage through conical intersections. *J. Chem. Phys.* **2006**, *125* (17), 174309.
(30) Lan, Z.; Dupays, A.; Vallet, V.; Mahapatra, S.; Domcke, W. Photoinduced multi-mode quantum dynamics of pyrrole at the $^1\pi\sigma^*$-S_0 conical intersections. *J. Photochem. Photobiol., A* **2007**, *190* (2−3), 177−189.
(31) Vallet, V.; Lan, Z. G.; Mahapatra, S.; Sobolewski, A. L.; Domcke, W. Photochemistry of pyrrole: Time-dependent quantum wave-packet description of the dynamics at the $^1\pi\sigma^*$-S_0 conical intersections. *J. Chem. Phys.* **2005**, *123* (14), 144307.
(32) Vallet, V.; Lan, Z.; Mahapatra, S.; Sobolewski, A. L.; Domcke, W. Time-dependent quantum wave-packet description of the $1\pi\sigma^*$ photochemistry of pyrrole. *Faraday Discuss.* **2004**, *127* (0), 283−293.
(33) Gaenko, A.; DeFusco, A.; Varganov, S. A.; Martínez, T. J.; Gordon, M. S. Interfacing the ab Initio multiple spawning method with electronic structure methods in GAMESS: Photodecay of trans-azomethane. *J. Phys. Chem. A* **2014**, *118* (46), 10902−10908.
(34) Perring, A. E.; Pusede, S. E.; Cohen, R. C. An observational perspective on the atmospheric impacts of alkyl and multifunctional nitrates on ozone and secondary organic aerosol. *Chem. Rev.* **2013**, *113* (8), 5848−5870.
(35) Williams, J. E.; Le Bras, G.; Kukui, A.; Ziereis, H.; Brenninkmeijer, C. A. M. The impact of the chemical production of methyl nitrate from the NO + CH_3O_2 reaction on the global distributions of alkyl nitrates, nitrogen oxides and tropospheric ozone: a global modelling study. *Atmos. Chem. Phys.* **2014**, *14* (5), 2363−2382.
(36) Yang, X.; Felder, P.; Huber, J. R. Photodissociation of methyl nitrate in a molecular beam. *J. Phys. Chem.* **1993**, *97* (42), 10903−10910.
(37) Chuck, A. L.; Turner, S. M.; Liss, P. S. Direct evidence for a marine source of C_1 and C_2 alkyl nitrates. *Science* **2002**, *297* (5584), 1151−1154.
(38) Soto, J.; Peláez, D.; Otero, J. C.; Avila, F. J.; Arenas, J. F. Photodissociation mechanism of methyl nitrate. A study with the multistate second-order multiconfigurational perturbation theory. *Phys. Chem. Chem. Phys.* **2009**, *11* (15), 2631−2639.
(39) Arenas, J. F.; Avila, F. J.; Otero, J. C.; Peláez, D.; Soto, J. Approach to the atmospheric chemistry of methyl nitrate and methylperoxy nitrite. Chemical mechanisms of their formation and decomposition reactions in the gas phase. *J. Phys. Chem. A* **2008**, *112* (2), 249−255.
(40) Carbajo, P. G.; Orr-Ewing, A. J. NO_2 quantum yields from ultraviolet photodissociation of methyl and isopropyl nitrate. *Phys. Chem. Chem. Phys.* **2010**, *12* (23), 6084−6091.
(41) Talukdar, R. K.; Burkholder, J. B.; Hunter, M.; Gilles, M. K.; Roberts, J. M.; Ravishankara, A. R. Atmospheric fate of several alkyl nitrates Part 2 UV absorption cross-sectionsand photodissociation quantum yields. *J. Chem. Soc., Faraday Trans.* **1997**, *93*, 2797−2805.
(42) Algarra, M.; Soto, J.; Pinto da Silva, L.; Pino-Gonzalez, M. S.; Rodriguez-Borges, J. E.; Mascetti, J.; Borget, F.; Reisi-Vanani, A.; Luque, R. Insights into the photodecomposition of azidomethyl methyl sulfide: a S_2/S_1 conical intersection on nitrene potential energy surfaces leading to the formation of S-methyl-N-sulfenylmethanimine. *J. Phys. Chem. A* **2020**, *124* (10), 1911−1921.
(43) Aranda, D.; Avila, F. J.; López-Tocón, I.; Arenas, J. F.; Otero, J. C.; Soto, J. An MS-CASPT2 study of the photodecomposition of 4-methoxyphenyl azide: role of internal conversion and intersystem crossing. *Phys. Chem. Chem. Phys.* **2018**, *20* (11), 7764−7771.
(44) Arenas, J. F.; Otero, J. C.; Peláez, D.; Soto, J. CASPT2 study of the decomposition of nitrosomethane and its tautomerization reactions in the ground and low-lying excited states. *J. Org. Chem.* **2006**, *71* (3), 983−991.
(45) Zhang, J.; Peng, J.; Hu, D.; Lan, Z. Investigation of nonadiabatic dynamics in the photolysis of methyl nitrate (CH_3ONO_2) by on-the-fly surface hopping simulation. *Phys. Chem. Chem. Phys.* **2021**, *23* (45), 25597−25611.
(46) Becke, A. D. Density-functional exchange-energy approximation with correct asymptotic behavior. *Physical Review A Gen.Phys.* **1988**, *38* (6), 3098−3100.
(47) Lee, C.; Yang, W.; Parr, R. G. Development of the Colle-Salvetti correlation-energy formula into a functional of the electron density. *Phys. Rev. B Condens.Matter.* **1988**, *37* (2), 785−789.
(48) Vosko, S. H.; Wilk, L.; Nusair, M. Accurate spin-dependent electron liquid correlation energies for local spin density calculations: a critical analysis. *Can. J. Phys.* **1980**, *58* (8), 1200−1211.
(49) Becke, A. D. Density-functional thermochemistry. III. The role of exact exchange. *J. Chem. Phys.* **1993**, *98* (7), 5648−5652.
(50) Frisch, M. J.; Trucks, G. W.; Schlegel, H. B.; Scuseria, G. E.; Robb, M. A.; Cheeseman, J. R.; Scalmani, G.; Barone, V.; Petersson, G. A.; Nakatsuji, H.; Li, X.; Caricato, M.; Marenich, A. V.; Bloino, J.; Janesko, B. G.; Gomperts, R.; Mennucci, B.; Hratchian, H. P.; Ortiz, J. V.; Izmaylov, A. F.; Sonnenberg, J. L.; Williams; Ding, F.; Lipparini, F.; Egidi, F.; Goings, J.; Peng, B.; Petrone, A.; Henderson, T.; Ranasinghe, D.; Zakrzewski, V. G.; Gao, J.; Rega, N.; Zheng, G.; Liang, W.; Hada, M.; Ehara, M.; Toyota, K.; Fukuda, R.; Hasegawa, J.; Ishida, M.; Nakajima, T.; Honda, Y.; Kitao, O.; Nakai, H.; Vreven, T.; Throssell, K.; Montgomery, J. A., Jr.; Peralta, J. E.; Ogliaro, F.; Bearpark, M. J.; Heyd, J. J.; Brothers, E. N.; Kudin, K. N.; Staroverov, V. N.; Keith, T. A.; Kobayashi, R.; Normand, J.; Raghavachari, K.; Rendell, A. P.; Burant, J. C.; Iyengar, S. S.; Tomasi, J.; Cossi, M.; Millam, J. M.; Klene, M.; Adamo, C.; Cammi, R.; Ochterski, J. W.;

https://doi.org/10.1021/acs.jpclett.3c00664
J. Phys. Chem. Lett. 2023, 14, 6542−6549

Martin, R. L.; Morokuma, K.; Farkas, O.; Foresman, J. B.; Fox, D. J. *Gaussian 16*, revision C.01; Gaussian: Wallingford, CT, 2016.
(51) Finley, J.; Malmqvist, P.-Å.; Roos, B. O.; Serrano-Andrés, L. The multi-state CASPT2 method. *Chem. Phys. Lett.* **1998**, *288* (2−4), 299−306.
(52) Granovsky, A. A. Extended multi-configuration quasi-degenerate perturbation theory: The new approach to multi-state multi-reference perturbation theory. *J. Chem. Phys.* **2011**, *134* (21), 214113.
(53) Shiozaki, T.; Győrffy, W.; Celani, P.; Werner, H.-J. Communication: Extended multi-state complete active space second-order perturbation theory: Energy and nuclear gradients. *J. Chem. Phys.* **2011**, *135* (8), 081106.
(54) Yarkony, D. R. On the adiabatic to diabatic states transformation near intersections of conical intersections. *J. Chem. Phys.* **2000**, *112* (5), 2111−2120.
(55) Müller, U.; Stock, G. Surface-hopping modeling of photo-induced relaxation dynamics on coupled potential-energy surfaces. *J. Chem. Phys.* **1997**, *107* (16), 6230−6245.
(56) Du, L.; Lan, Z. An on-the-fly surface-hopping program JADE for nonadiabatic molecular dynamics of polyatomic systems: Implementation and applications. *J. Chem. Theory Comput.* **2015**, *11* (4), 1360−1374.
(57) Tully, J. C. Molecular dynamics with electronic transitions. *J. Chem. Phys.* **1990**, *93* (2), 1061−1071.
(58) Shiozaki, T. BAGEL: brilliantly advanced general electronic-structure library. *Wiley Interdiscip. Rev.: Comput. Mol. Sci.* **2018**, *8* (1), e1331.
(59) Barbatti, M.; Pittner, J.; Pederzoli, M.; Werner, U.; Mitrić, R.; Bonačić-Koutecký, V.; Lischka, H. Non-adiabatic dynamics of pyrrole: Dependence of deactivation mechanisms on the excitation energy. *Chem. Phys.* **2010**, *375* (1), 26−34.
(60) Barbatti, M.; Granucci, G.; Persico, M.; Ruckenbauer, M.; Vazdar, M.; Eckert-Maksić, M.; Lischka, H. The on-the-fly surface-hopping program system Newton-X: Application to ab initio simulation of the nonadiabatic photodynamics of benchmark systems. *J. Photochem. Photobiol.A* **2007**, *190* (2), 228−240.
(61) Prlj, A.; Ibele, L. M.; Marsili, E.; Curchod, B. F. E. On the theoretical determination of photolysis properties for atmospheric volatile organic compounds. *J. Phys. Chem. Lett.* **2020**, *11* (14), 5418−5425.
(62) Blancafort, L.; Jolibois, F.; Olivucci, M.; Robb, M. A. Potential energy surface crossings and the mechanistic spectrum for intramolecular electron transfer in organic radical cations. *J. Am. Chem. Soc.* **2001**, *123* (4), 722−732.
(63) Yue, L.; Liu, Y.-J. Conical intersection in chemiluminescence of cyclic peroxides. *J. Phys. Chem. Lett.* **2022**, *13* (46), 10671−10687.
(64) Granucci, G.; Persico, M. Critical appraisal of the fewest switches algorithm for surface hopping. *J. Chem. Phys.* **2007**, *126* (13), 134114.
(65) Subotnik, J. E.; Shenvi, N. A new approach to decoherence and momentum rescaling in the surface hopping algorithm. *J. Chem. Phys.* **2011**, *134* (2), 024105.
(66) Landry, B. R.; Subotnik, J. E. How to recover Marcus theory with fewest switches surface hopping: Add just a touch of decoherence. *J. Chem. Phys.* **2012**, *137* (22), 22A513.
(67) Subotnik, J. E.; Ouyang, W.; Landry, B. R. Can we derive Tully's surface-hopping algorithm from the semiclassical quantum Liouville equation? Almost, but only with decoherence. *J. Chem. Phys.* **2013**, *139* (21), 214107.
(68) Jain, A.; Alguire, E.; Subotnik, J. E. An efficient, augmented surface hopping algorithm that includes decoherence for use in large-scale simulations. *J. Chem. Theory Comput.* **2016**, *12* (11), 5256−5268.
(69) Subotnik, J. E.; Jain, A.; Landry, B.; Petit, A.; Ouyang, W.; Bellonzi, N. Understanding the surface hopping view of electronic transitions and decoherence. *Annu. Rev. Phys. Chem.* **2016**, *67* (1), 387−417.
(70) Mai, S.; Marquetand, P.; González, L. Nonadiabatic dynamics: The SHARC approach. *Wiley Interdiscip. Rev.: Comput. Mol. Sci.* **2018**, *8* (6), e1370.

https://doi.org/10.1021/acs.jpclett.3c00664
J. Phys. Chem. Lett. 2023, 14, 6542−6549